inorganics

Article

Complexes of Ni^{II}, Co^{II}, Zn^{II}, and Cu^{II} with Promising Anti-Tuberculosis Drug: Solid-State Structures and DFT Calculations

Mohamed Ali Ahmed, Maksim A. Zhernakov, Edward M. Gilyazetdinov, Mikhail S. Bukharov, Daut R. Islamov, Konstantin S. Usachev, Alexander E. Klimovitskii, Nikita Yu. Serov, Vladimir A. Burilov and Valery G. Shtyrlin

Article

Complexes of Ni^{II}, Co^{II}, Zn^{II}, and Cu^{II} with Promising Anti-Tuberculosis Drug: Solid-State Structures and DFT Calculations

Mohamed Ali Ahmed [1,2], Maksim A. Zhernakov [1], Edward M. Gilyazetdinov [1], Mikhail S. Bukharov [1], Daut R. Islamov [1,3], Konstantin S. Usachev [3], Alexander E. Klimovitskii [1], Nikita Yu. Serov [1], Vladimir A. Burilov [1] and Valery G. Shtyrlin [1,*]

[1] A. M. Butlerov Chemistry Institute, Kazan Federal University, Kremlevskaya St., 18, Kazan 420008, Russia
[2] Chemistry Department, Faculty of Science, Damanhour University, Damanhour 22511, Egypt
[3] Laboratory for Structural Analysis of Biomacromolecules, Kazan Scientific Center of Russian Academy of Science, Kremlevskaya St., 31, Kazan 420008, Russia
[*] Correspondence: valery.shtrylin@gmail.com

Abstract: Four new Ni^{II}, Co^{II}, Zn^{II}, and Cu^{II} complexes with the promising anti-tuberculosis drug (*E/Z*)-N′-((5-Hydroxy-3,4-bis(hydroxymethyl)-6-methylpyridin-2-yl)methylene)-isonicotino-hydrazide (**LH**) were synthesized and characterized by structural methods: single-crystal X-ray diffraction, vibrational spectroscopy, and mass spectrometry. The Ni^{II}, Co^{II}, and Zn^{II} metal ions form only amorphous phases with various morphologies according to mass spectrometry and IR spectroscopy. The Cu^{II} forms a crystalline 1D coordination polymer with the relative formula $\frac{1}{\infty}\{[CuLCl]\cdot 0.5H_2O\}$. Even though the **LH** ligand in the crystalline state includes a mixture of *E*-/*Z*-isomers, only the tautomeric iminol *E*-/*Z*-form is coordinated by Cu^{II} in the crystal. The copper(II) complex crystallizes in the monoclinic *P*2$_1$/*n* space group with the corresponding cell parameters a = 16.3539(11) Å, b = 12.2647(6) Å, and c = 17.4916(10) Å; α = 90°, β = 108.431(7)°, and γ = 90°. DFT calculations showed that the *Z*-isomer of the **LH** ligand in solution has the lowest formation energy due to intramolecular hydrogen bonds. According to the quantum chemical calculations, the coordination environment of the Cu^{II} atom during the transfer of the molecule into the solution remains the same as in the crystal, except for the polymeric bond, namely, distorted trigonal bipyramidal. Some of the complexes investigated can be used as effective sensors in biosystems.

Keywords: coordination compounds; hydrazones; *d*-metals; tuberculosis; structures; DFT calculations

1. Introduction

Although tuberculosis has been known for hundreds of years, there is still a need for effective drug treatment, as the alarming emergence of multidrug-resistant strains of *Mycobacterium tuberculosis* (Mtb) has led the scientific community to seek new effective anti-tuberculosis drugs. Some hydrazones are biologically active compounds. These molecules can be obtained by condensing isonicotinehydrazide with pharmacologically active carbonyl molecules to create prospective anti-TB drugs, such as pyridoxal isonicotinoyl hydrazine (PIH) [1–6].

The crucial role of *d*-metals in biosystems is well known as they form coordination centers in metalloproteins and enzymes, bind organic and inorganic molecules, control reaction rates, and enhance drug activity [7–9]. Therefore, the coordination chemistry of aroylhydrazone complexes with vital metals has received much attention due to their versatile ability to bind to the complexes and potential pharmacological applications [10–13]. Meanwhile, *f*-metals have no significant biological importance; their complexes with various types of ligands, including hydrazones, have been widely studied as they can be effective sensors, NIR emitters, and luminescent thermometers [14–16]. Depending on the substituents,

metal ion, and reaction conditions, aroylhydrazones with multiple coordination centers can function as neutral, anionic, bidentate, or tridentate ligands in keto- or enol-tautomeric forms [12,13,17–20].

The anti-tubercular activity of Co(II), Ni(II), Cu(II), and Zn(II) complexes is higher than that of the parent ligand (salicyl-hydrazone). The anti-TB activity of the Co(II) complex against *Mycobacterium tuberculosis* H37Rv is equipotent to the standard drug isoniazid [20]. The antimicrobial activity of aroylhydrazone and Mn(II), Fe(II), Ni(II), Cu(II), and V(II) complexes against *M. tuberculosis* H37Rv was also established, and their potency level was compared with isoniazid [21]. The results obtained indicated that the metal complexes are more active than isoniazid itself. Metals that are out of place in the organism can also be found in the form of central ions; for example, palladium(II) [19] and gold(III) [22] complexes with modified hydrazones are being worked on.

In addition to studying the solid-state structure, it is necessary to know the behavior of *d*-metal cations and hydrazones in solutions. The stability constants of the Cu(II), Zn(II), and Au(III) complexes with isonicotinoyl hydrazone derivatives (pyridine-2-, -3-, and 4-carbohydrazones of pyridoxal-5-phosphate) were determined using titration. Cu(II) ions formed more stable *bis*-complexes than Zn(II), whereas zinc (II) ions easily bound to the picolinic acid hydrazone derivative to form a 1:1 complex [10,11,22].

It was found that the newly synthesized compound (*E/Z*)-N′-((5-Hydroxy-3,4-bis(hydroxymethyl)-6-methylpyridin-2-yl)methylene)-isonicotinohydrazide (**LH**) [23] showed outstanding antimycobacterial activity against all strains whose MDR profile comprised first- and second-line medicines, and it was more effective than PIH against the *M. tuberculosis* H37Rv strain. Human cells used in cytotoxicity assays of **LH** revealed that it is 1.5–2 times less harmful than ethambutol and moxifloxacin and 2–3 times less toxic than isoniazid. The **LH** ligand exhibited weak complexation with Fe^{3+} ions, minimal acute toxicity (LD_{50} > 2.000 mg/kg *per os* in mice), and efficacy in a mouse model of drug-sensitive tuberculosis comparable to that of isoniazid and considerably superior to that of ethambutol and moxifloxacin [23].

This study is on the Co^{II}, Ni^{II}, Zn^{II}, and Cu^{II} complexes with **LH**, because it is urgent to know how this promising anti-TB drug interacts with these crucial micro-elements, without which human well-being is impossible. It should be specially emphasized that complexes of transition metals with hydrazone derivatives can act as effective sensors, in particular in biosystems [24,25].

2. Results and Discussion

2.1. Synthesis and Structural Analysis

Since **LH** is the condensation product of an aldehyde and a hydrazide, it has great potential for isomerism and tautomerism (Figure 1). The synthetic method yields ligands in *E*-/*Z*-forms with a 2:1 ratio [23], and this mixture was used to synthesize the complexes. During the research, it was found that ligand is specific because of several reasons. Firstly, the amide form of **LH** contains only weak and individual donors, so a chelate cycle cannot be formed; secondly, a chelate cycle can be formed if the pyridoxine fragment is flipped, but the rotation is inhibited by the presence of two methoxy groups; and thirdly, hydrazone/iminol equilibrium is shifted to the right in the presence of alkali, but hydrazone may undergo hydrolysis to pyridoxine and isonicotine in alkaline medium. A possible isomerization mechanism is shown in Figure S3: there is an equilibrium between the *E*- and *Z*-forms of the ligand in solution, which can be shifted towards the formation of the *E*-form, for example via complex formation. After that, only a proton shift is required, causing the hydrazone/iminol tautomerism. Then, a rotation around the selected C-C and C-N bonds in the resonance structures can occur, leading to the **LH** form required for complexation.
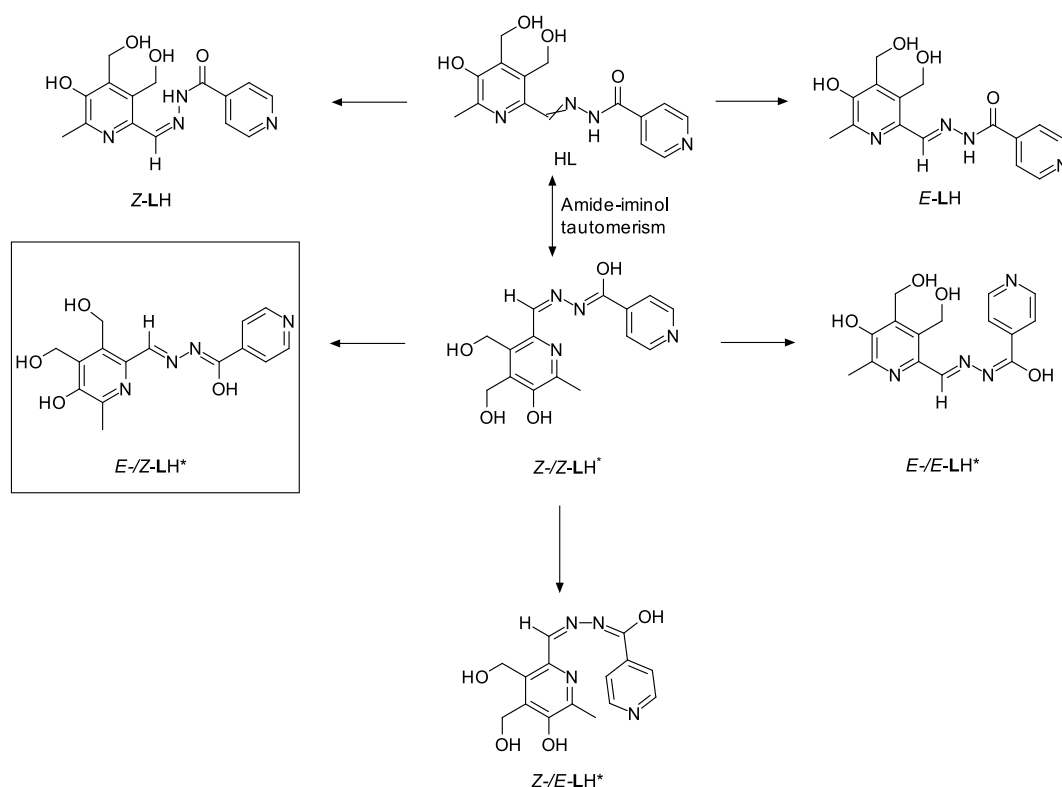
Figure 1. Isomerism of the **LH** ligand. **LH*** – ligand conformers designation.

The above explains why **LH** does not form solid-state complexes of Ni^{2+}, Co^{2+}, and Zn^{2+} but amorphous ones (Scheme 1), as the alkaline medium, which is required to create iminol, also leads to the partial hydrolysis of metal ions. From statistical considerations, forming *E-/Z*-tautomeric iminol is hampered due to the multistep process of compounding and rotation around the $C_{pyridoxine}$–C_{imine} bond, although this form is probably the most stable due to the minimal repulsion of the substituents at the double bonds (see DFT calculations below). Cu^{2+}, unlike the others, is a Jahn–Teller ion [26], resulting in its high reactivity in solution, so the energy gain after complexation with **LH** can overlap the energy demands of tautomeric transformation and conformational alterations.
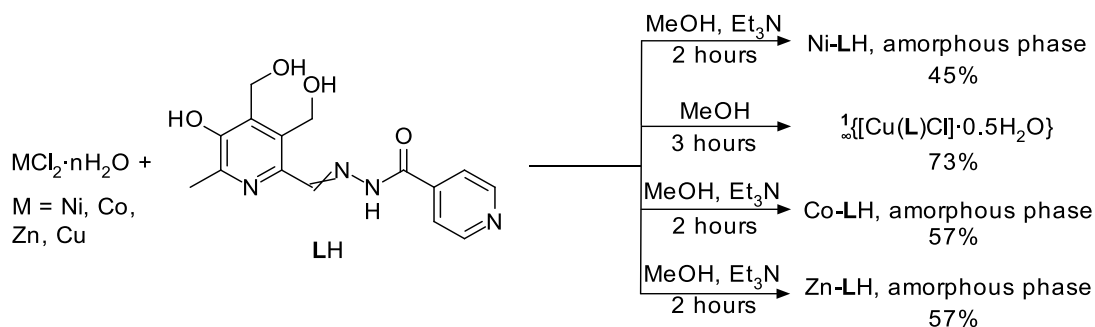
Scheme 1. Synthetic route of the corresponding complexes.

The copper(II) complex with its respective ligand is a one-dimensional (1D) coordination polymer, which crystallizes in the monoclinic $P2_1/n$ (#14) space group, and the unit cell has eight structural units (Figure 2a). The Cu^{2+} central ion has a coordination number of five (Figure 2b), since it coordinates the pyridine and hydrazine nitrogen atoms, as well as the hydroxyl group, of one **LH** molecule, chloride ion, and pyridine nitrogen atom from another molecule, leading to polymer chain growth along the b axis.
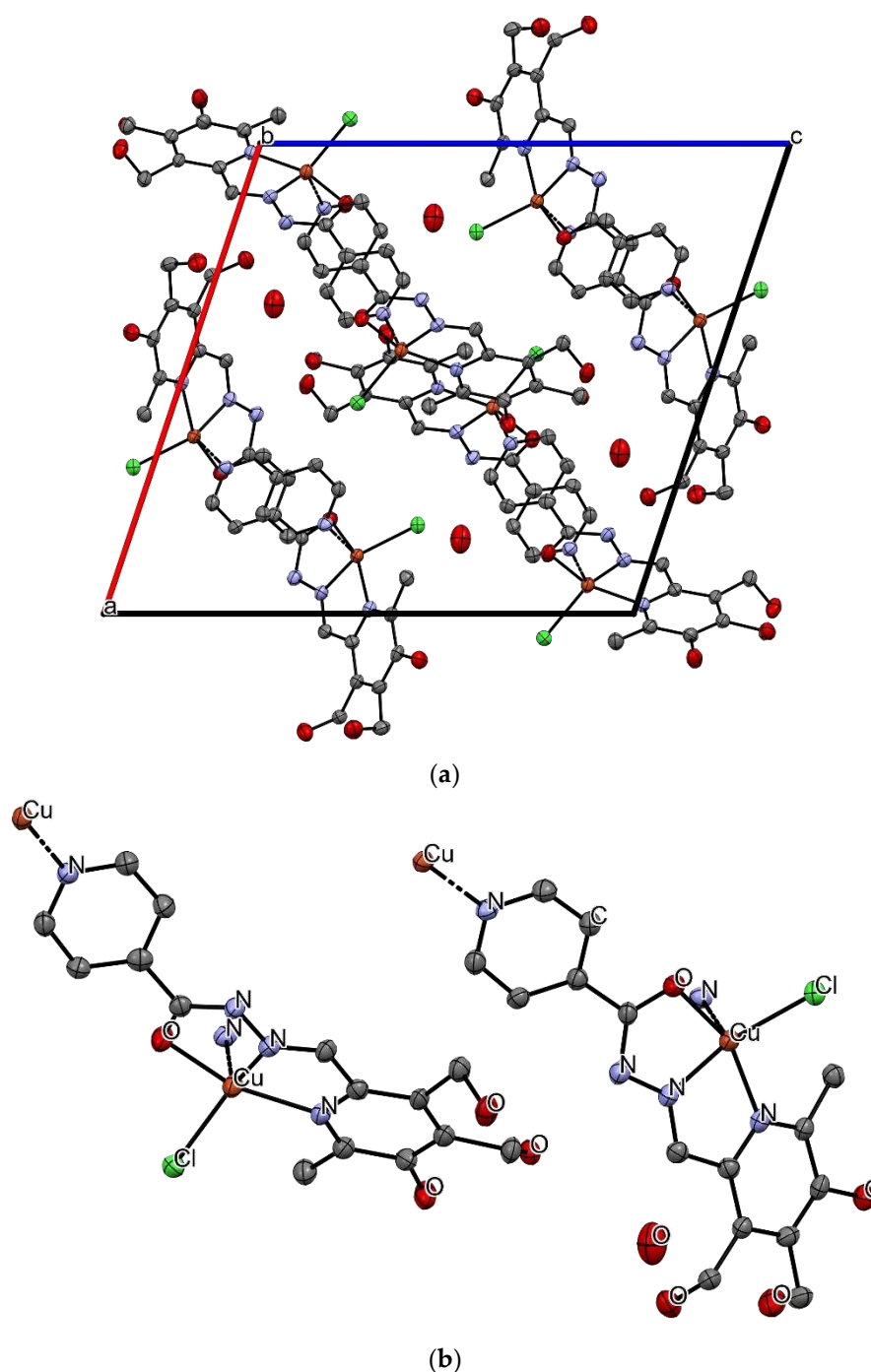
(**a**)

(**b**)

Figure 2. (**a**) View of a unit cell along the b axis of the corresponding crystal structure. (**b**) Complex unit of $\frac{1}{\infty}\{[\text{Cu}\mathbf{L}\text{Cl}]\cdot 0.5\text{H}_2\text{O}\}$. Thermal ellipsoids describe a 50% probability level of atoms; hydrogen atoms are omitted for clarity. The dashed Cu–N bond is a polymeric one.

The coordinated atoms form a disordered trigonal bipyramid, which is truly unique to copper(II) complexes with non-tripod ligands and more likely for Cu^{I} [8,27,28]. Usually in complexes with hydrazones, the Cu^{II} ion has a disordered square pyramidal environment (Figure 3), which is consistent with the concept of the Jahn–Teller effect [12,17,20,24]. There are two symmetrically inequivalent copper atoms in the unit cell, Cu1A and Cu1B, so the distances between atoms coordinated to them are different. Cu1A and Cu1B interatomic distances between N$_{\text{pyridine}}$, Cl, O, N$_{\text{hydrazide}}$, and N$_{\text{polymeric}}$ are shown in Table 1. The Cu-Cl distance is the longest; the other four are close enough in value, and that generally corresponds to a distorted square pyramid. However, the values of the valence angles are

closer to the trigonal bipyramid: $N_{16A(hydrazide)}$–Cu–Cl is 140.13°, N_{16A}–Cu–$N_{23A(polymeric)}$ is 146.86°, $N_{polymeric}$–Cu–Cl is 101.41°, O–Cu–$N_{3A(pyridine)}$ is 158.02°, O–Cu–$N_{hydrazide}$ 78.66°, O–Cu–Cl 91.82°, O–Cu–$N_{polymeric}$ 89.14°, $N_{pyridine}$–Cu–Cl 106.96°, $N_{pyridine}$–Cu–$N_{hydrazide}$ 79.58°, and $N_{pyridine}$–Cu–$N_{polymeric}$ 97.97°. According to this, the oxygen and $N_{pyridine}$ atoms are in the "axial" position, and Cl, $N_{hydrazide}$, and $N_{polymeric}$ are in the relative "equatorial" position. The results obtained are consistent with the theoretical concepts of the Jahn–Teller pseudo-effect predicted for fast transitions between isomers of copper(II) complexes [29,30].
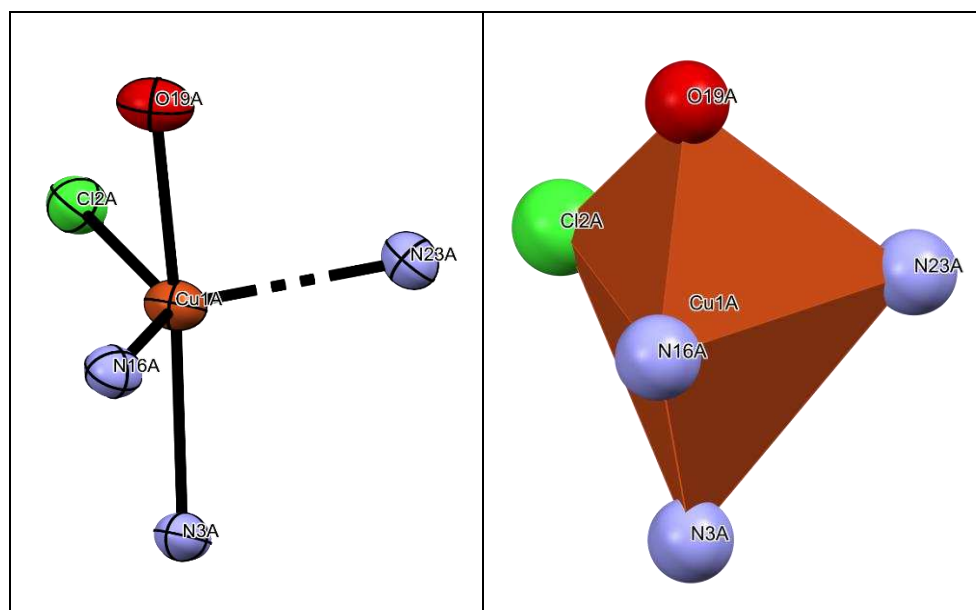

Figure 3. Coordination polyhedron around Cu^{2+} ion in the $^1_\infty\{[\mathbf{CuLCl}]\cdot0.5H_2O\}$ complex.

Table 1. Selected interatomic distances of $^1_\infty\{[\mathbf{CuLCl}]\cdot0.5H_2O\}$.

Atom	Cu1A	Cu1B
$N_{pyridine}$	2.073(4) Å	2.079(5) Å
Cl	2.280(2) Å	2.248(2) Å
O	2.043(4) Å	2.035(4) Å
$N_{hydrazide}$	1.922(4) Å	1.941(4) Å
$N_{polymeric}$	2.134(5) Å	2.150(4) Å

Since the **LH** ligand is a potential drug, it will be necessary to find out the mechanism of its liberation, which requires laborious experiments. Nevertheless, from general considerations, the following mechanism can be proposed: Cu^{II} has a high rate of ligand exchange in solution [26,29,30], and the concentration of the injected complex is usually low. In this case, **LH** will be substituted either by H_2O molecules or amino acids in the body, which will result in the formation of a free ligand. However, a significant drawback of hydrazone derivatives (particularly PIH) is known to be the removal of important ions such as $Fe^{2+/3+}$ from cells [1,23]. The copper(II) complex presented may not have this disadvantage due to the strong binding of the ligand to the metal. It also cannot be denied that the copper(II) complex itself may exhibit anti-TB activity.

Previously (Figure 1), it has been shown that **LH** has many spatial isomers and conformers and two tautomeric forms. Interestingly, for synthesis, we used an isomer mixture of hydrazone with a 2:1 *E/Z* ratio but only iminol in the *E-/Z*-form crystallized (Figure 1, structure in the brackets). Since the reaction was performed in CH_3OH without alkali, we can claim that Cu^{II} not only shifts the equilibrium towards iminol by complexation but also

gives a stereoselective product, unlike other *d*-metals, which probably cannot react with LH in an alkali-free medium.

A geometry check with "Mogul" [31] was performed to determine deviations from the trends in the complex reported, and four interatomic distance values were marked as "unusual": Cu–N$_{pyridine}$, Cu–Cl, Cu–O, and C–O$_{carbonyl}$ (1.262(7) Å), but Cu–N$_{polymeric}$ had no matches within the CCDC database. The Cu–N$_{pyridine}$ interatomic distance in similar structures has a range of 1.970–2.056 Å with a mean value of 2.022 Å [17,32–34], Cu–Cl has a range of 1.939–2.724 Å with a mean of 2.518 Å [17,33], Cu–O has a range of 1.918–1.983 Å with a mean of 1.951 Å [35], and C–O has a range of 1.234–1.326 Å with a mean of 1.288 Å [12,36]. These deviations can be explained by the fact that the isonicotinic fragment moves out of the plane of the rest of the molecule by ~35° (Figure S1), because the nitrogen atom is responsible for the growth of the polymer chain, while the oxygen atom of the deprotonated OH group, formed due to tautomerism, coordinates the copper(II), which is at an unusually large distance from the oxygen atom.

The Cu1A–N$_{polymeric}$ and Cu1B–N$_{polymeric}$ bonds form two polymer chains (Figure 4), which produce "herringbones" inverted relative to each other and connected by a system of intermolecular hydrogen bonds between the H atoms in the methoxy group and hydrazide N atom (Figure S2). These contacts are rather short (1.856 Å and 1.875 Å, respectively), so it is obvious that they influence the relative orientation and crystal packing.
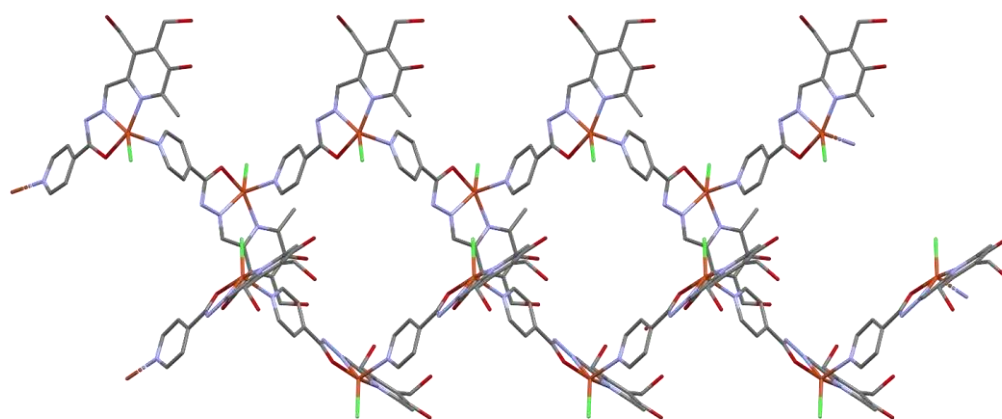

Figure 4. Polymeric expansion of $^1_\infty\{[CuLCl]\cdot0.5H_2O\}$ along the a axis. Cu—brown, Cl—green, N—blue, O—red, C—grey. H atoms are omitted for clarity.

2.2. Mass Spectrometry

As it was not possible to obtain cobalt(II), nickel(II), and zinc(II) complexes in the crystalline state, they were analyzed by high-resolution ESI-MS to confirm the ligand binding and determine the molecular weight.

Thus, the most intense peak for the Co-LH complex was found at *m/z* = 689.1517 (Figure S4). The calculated molecular weight of the cobalt *bis*-complex $C_{30}H_{30}CoN_8O_8$ is 689.1519; therefore, it can be stated that the [Co**L**$_2$] structure is real.

For the Ni-**LH** complex, it was found that the most intense peaks are the protonated ligand itself (found at *m/z* = 317.1248 (Figure S5); the calculated molecular weight of $C_{15}H_{17}N_4O_4$ is 317.1244) and the ligand acetonitrile solvate (found at *m/z* = 357.1561; the calculated molecular weight of $C_{15}H_{16}N_4O_4\cdot C_2H_3N$ is 357.1431). The two heaviest *m/z* peaks are 411.0171 and 409.0212, indicating that the molecular ion contains a Cl atom, as it is represented in nature by two isotopes, 35 and 37. The calculated molecular weight of $C_{15}H_{16}ClN_4NiO_4$ is 409.0208, and it can be stated that the [Ni**L**Cl] structure is real.

For the Zn-**LH** complex, the most intense peak was found at *m/z* = 396.2113 (Figure S6). The calculated molecular weight of $C_{15}H_{16}N_4O_5Zn$ representing the hydroxo-complex [Zn**L**(OH)] is 396.0423. The peak *m/z* = 663.4547 corresponds to the ligand dimer methanol solvate (the calculated m/z ratio of $C_{31}H_{35}N_8O_9$ is 663.2532). The biggest *m/z* ratio of

764.5744 could correspond to the molecule $C_{15}H_{23}N_4O_{11}ClZn_4K$ (calculated m/z = 764.7898), representing the possible structure $K[Zn_4L(OH)_6Cl]\cdot H_2O$.

In high-resolution mass spectroscopy, a structure can be considered real if the relative error is around 0.01%. It was performed for the Co^{II} and Ni^{II} structures with errors of around 0.003%, while for the corresponding Zn^{II} structures, they were 0.03% for both supposed molecules.

2.3. IR Spectroscopy

In the IR spectrum of **LH** in the solid state, a strong band at 1640 cm^{-1} is observed, which can be attributed to carbonyl groups (Figure 5). Such a shift can be explained by the conjugation with double bonds and an aromatic system, and an intermolecular H bond, which can be realized in the Z-isomer. Narrow peaks at 1257 cm^{-1} (ν_{Ar-OH}) and 1077 cm^{-1} show the presence of a hydroxyl group (ν_{CH2-OH}). An intramolecular hydrogen bond (N···HO), as well as crystalline H_2O, are responsible for the broad band between 3250 and 3450 cm^{-1}. Because of the presence of the group (-CH=N-NH-C(=O)–), the **LH** ligand can exhibit hydrazone–iminol tautomerism. The presence of a strong signal characteristic of the vibrations of the C=O group and the absence of a band which could be attributed to ν(=C-OH) in the spectra of the free ligand indicate that the hydrazone stabilizes the keto-tautomeric form, and it was also proved by single-crystal X-ray diffraction [23]. The doublet band with maxima at 1579 cm^{-1} and 1549 cm^{-1} corresponds to the valence vibrations of the azomethine molecule (C=N) and the skeletal (C-C) vibrations of the aromatic rings. Due to the joint effect of the mode of stretching vibrations of the N-C=O group and the N-H bond strain, the signal is recorded at 1430 cm^{-1}. The broad bands in the complexes' spectra can be explained by the presence of crystalline water and a large number of hydrogen bonds, which complicates their interpretation. However, the disappearance of the amide and carbonyl bands is observed for Cu^{II}, Ni^{II}, and Zn^{II} complexes, showing the loss of the hydrazide proton as a result of complexation with the metal ion, which refers to the ligand coordination in the iminol form [37]. For the Co^{II} complex, a strong band at 1640 cm^{-1} is also observed, indicating that the bond between the central ion and the ligand occurs either via hydrazide nitrogen or carbonyl oxygen, which corresponds to the constitution of the *bis*-complex which was detected by high-resolution ESI-MS.
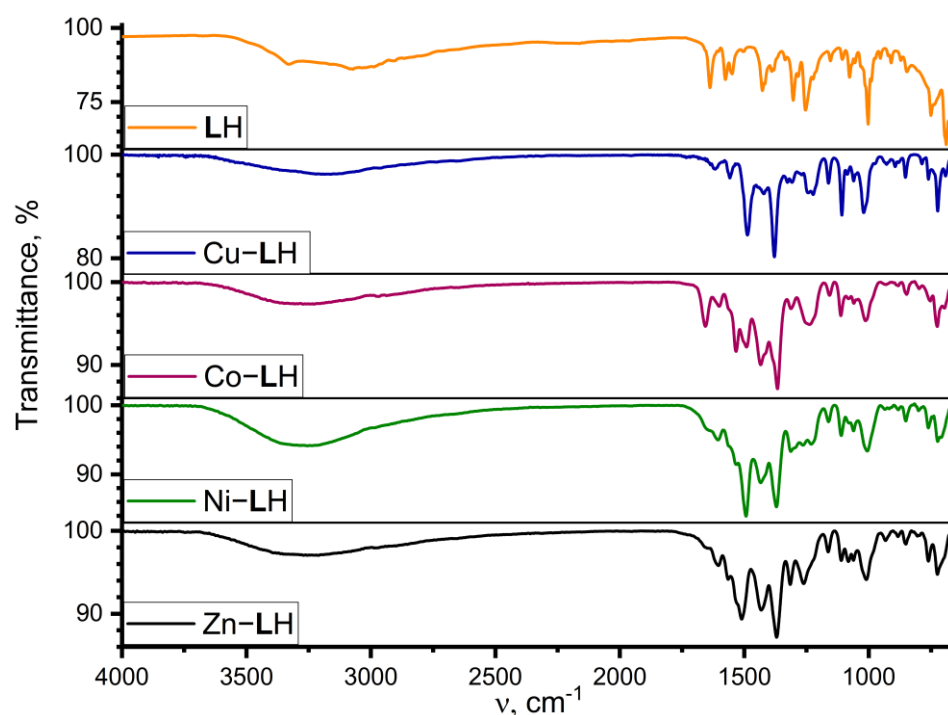

Figure 5. Solidstate IR spectra of the title compounds.

2.4. Quantum Chemical Calculations

Studying the structure of a solid is necessary, but it gives no unambiguous insight into how the system will behave in solution. The classical method for determining the composition in solutions is titration, but with the development of computing power, it is possible to estimate the stability and parameters of the molecule when it is moved to a solvent medium [38–40]. Thus, we can estimate which **L**H isomer is more stable in solution and therefore explain why only one form is coordinated and how it will change the distances between the Cu^{II} and coordinated atoms.

The optimized structures and formation energies of **L**H *E*- and *Z*-isomers (Figures S7–S11) were calculated with ORCA [41] using the DFT method [42] on the B3LYP/def2-TZVPP level, accounting for solvent effects in the C-PCM model and dispersion correction (D3BJ). According to the calculations, the *Z*-isomer has a lower energy of formation when it corresponds to the conformer with an intermolecular hydrogen bond between $N_{pyridine}$ and the H atom, which is bound with $N_{hydrazine}$ (the energy comparison of the isomers is shown in Table 2). Even so, only the *E*-isomer is capable of chelate coordination, so there must be isomeric conversions in the solution.

Table 2. Selected interatomic distances of $^1_\infty\{[CuLCl]\cdot0.5H_2O\}$.

Isomer	Energy Difference, ΔE
Z-**L**H (Figure S8)	0
E-**L**H (Figure S7)	12.76 kJ/mol
Z-**L**H$^\beta$ (Figure S9)	10.58 kJ/mol
Z-**L**H$^\gamma$ (Figure S10)	17.43 kJ/mol
Z-**L**H$^\Delta$ (Figure S11)	28.41 kJ/mol

To compare the coordination sphere of the copper(II) complex in the solid phase and in solution, DFT calculations were performed taking into account the effects of the solvent (H_2O). The Cu-**L**H transfer into the solution remained a disordered trigonal bipyramid configuration (Figure 6), but the N-polymer atom was replaced by water molecules, as the existence of the coordination polymer in the solution is questionable. Our experience in quantum chemical calculations of transition metal complexes shows that, with appropriate functional and basis levels of calculations, the coordination sphere may significantly diverge from the one originally set for the calculation, even up to the loss of one of the coordinated groups even when using the C-PCM model [9,38–40]. Small variations in the interatomic distances are also present. Thus, concerning the copper atom, the chlorine and oxygen atoms become closer (2.276 Å instead of 2.280 Å and 2.035 instead of 2.043 Å, respectively); the pyridine and hydrazide nitrogen atoms become farther apart (2.129 Å instead of 2.073 Å and 1.955 Å instead of 1.922 Å, respectively); and the embedded "axial" water molecule is farthest away from it, making the surroundings become more like a square pyramid, but the chlorine atom is still outside the base plane. The replacement of the chlorine ion with a second water molecule is justified, because in solution Cl⁻ can be substituted by water molecules, since Cu^{II} has a high ligand exchange rate [26,29,40], which can reach values of about ~10^9 s^{-1} [30]; therefore, this phenomenon in solution is quite expected. This leads to a shorter Cu–X distance (2.052 Å (X = O_{water}) relative to 2.276 Å (X = Cl⁻)).
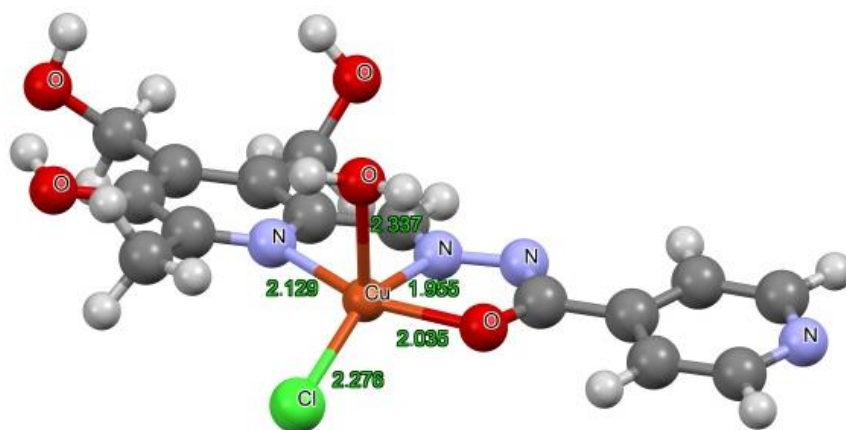
Figure 6. Structure of the [Cu**L**(H$_2$O)Cl] complex optimized on the B3LYP/def2-TZVPP level, accounting for solvent effects in the C-PCM model and dispersion correction (D3BJ).

3. Materials and Methods

3.1. Analytical Methods

- Single-crystal X-ray diffraction

The data set for the single crystal $^{1}_{\infty}$\{[Cu**L**Cl]·0.5H$_2$O\} was collected on a Rigaku XtaLab Synergy S instrument with a HyPix detector and a PhotonJet microfocus X-ray tube using Cu$_{K\alpha}$ (1.54184 Å) radiation at cryogenic temperature. Images were indexed and integrated using the CrysAlisPro data reduction package. Data were corrected for systematic errors and absorption using the ABSPACK module: numerical absorption correction based on Gaussian integration over a multifaceted crystal model and empirical absorption correction based on spherical harmonics according to the point group symmetry using equivalent reflections. The GRAL module was used for the analysis of systematic absences and space group determination. The structures were solved by direct methods using SHELXT [43] and refined by the full-matrix least squares method on F^2 using SHELXL [44]. Non-hydrogen atoms were refined anisotropically. The hydrogen atoms were inserted at the calculated positions and refined as riding atoms. The positions of the hydrogen atoms of methyl groups were found using rotating group refinement with idealized tetrahedral angles. The figures were generated using Mercury 4.1 program [45].

- IR spectroscopy

The FTIR spectra (600–4000 cm^{-1}) of solid samples were recorded on a Vertex 70 FTIR spectrometer (Bruker Corporation, Billerica, MA, USA) equipped with an ATR accessory (ZnSe crystal, MIRacle, PIKE Technologies, Madison, WI, USA). The background spectra obtained from 128 scans with a resolution of 2 cm^{-1} were subtracted from the spectra of the samples.

- Mass spectrometry

High-resolution mass spectra with electrospray ionization (HRESI MS) were obtained on an Agilent iFunnel 6550 Q-TOF LC/MS (Agilent Technologies, Santa Clara CA, USA) in positive mode. Carrier gas: nitrogen, temperature: 300 °C, carrier flow rate: 12 L·min^{-1}, nebulizer pressure: 275 kPa, funnel voltage: 3500 V, capillary voltage: 500 V, total ion current recording mode: 100–3000 *m/z* mass range, scanning speed: 7 spectra·s^{-1}. The sample was dissolved in a mixture of HPLC-MS acetonitrile/water in a ratio of 1:1, and the solution was supplied in HPLC-MS-grade methanol.

- DFT calculations

Structures of the ligand and copper complex were optimized with the ORCA program [41] using the DFT method [42] on the B3LYP/def2-TZVPP level [46–50], accounting

for the solvent effect (H_2O) by the C-PCM model [51] and the atom-pairwise dispersion correction with the Becke–Johnson damping scheme (D3BJ) [52,53]. All optimized structures were checked for the absence of imaginary frequencies.

3.2. Synthesis and Analytical Data

- General data

All synthetic work was performed under atmospheric conditions; the synthetic representation was made with MarvinSketch 21.20. Details on the crystallographic data, additional figures, computational parameters, and detailed mass spectra can be found in the supporting information for this article. CCDC 2249594 for $_\infty^1\{[CuLCl]\cdot 0.5H_2O\}$ contains the supplementary crystallographic data of this paper. These data can be obtained free of charge from The Cambridge Crystallographic Data Centre.

- Starting materials

(*E/Z*)-N′-((5-Hydroxy-3,4-bis(hydroxymethyl)-6-methylpyridin-2-yl)methylene)-isonicotino-hydrazide was prepared according to the literature method [22]. $CuCl_2\cdot 2H_2O$ (99.9%, Vekton Ltd., Saint Petersburg, Russia), $NiCl_2\cdot 6H_2O$ (99.9%, Vekton Ltd., Saint Petersburg, Russia), $CoCl_2\cdot 6H_2O$ (99.9%, Vekton Ltd., Saint Petersburg, Russia), $ZnCl_2$ (99.9%, Vekton Ltd., Saint Petersburg, Russia), CH_3OH (99%, Vekton Ltd., Saint Petersburg, Russia), and Et_2O (99%, Vekton Ltd., Saint Petersburg, Russia) were used as is. The Et_3N base was distilled and absolute according to the literature method.

- Synthesis of solid-state complexes

$_\infty^1\{[CuLCl]\cdot 0.5H_2O\}$

The complex was obtained by the following method: 31.6 mg (0.1 mmol) of **LH** was dissolved in 10 mL of methanol and then added to a 10 mL methanol solution of $CuCl_2\cdot 2H_2O$ (17.0 mg, 0.1 mmol). The mixture was stirred at room temperature for 3 h to give a pale brown precipitate. Afterwards, the mixture was filtered off, and the residue was washed with Et_2O and left to dry in air.

M^{II}-**LH** (M = Ni, Co, Zn)
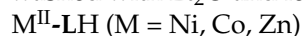
A methanol solution (10 mL) of respective $MCl_2\cdot nH_2O$ (0.1 mmol) was added to a methanol solution (10 mL) of **LH** (0.1 mmol) with a few drops of triethylamine. The mixture was refluxed for 2 h to ensure the complete precipitation of the formed substances. The amorphous complexes obtained were filtered off and washed several times with hot ethanol–methanol solution (1:1). Finally, the complexes obtained were washed with Et_2O and dried in vacuum desiccators over anhydrous $CaCl_2$.

Co–**LH**—reddish-brown powder. Yield: 57% based on $CoCl_2\cdot 6H_2O$;
Ni-**LH**—greenish-yellow powder. Yield: 45% based on $NiCl_2\cdot 6H_2O$;
Zn-**LH**—yellow powder. Yield: 57% based on $ZnCl_2$;
$_\infty^1\{[CuLCl]\cdot 0.5H_2O\}$—pale brown powder. Yield: 73% based on $CuCl_2\cdot 2H_2O$.

- Single crystal synthesis

A single crystal of $_\infty^1\{[CuLCl]\cdot 0.5H_2O\}$ was obtained by the following method: 31.6 mg, 0.1 mmol of **LH** was dissolved in 10 mL of methanol and then added to a 10 mL methanol solution of $CuCl_2\cdot 2H_2O$ (17.0 mg, 0.1 mmol). The mixture was stirred at room temperature for 1 h to give a pale brown solution. The solution was then left to evaporate slowly in air, and after 3 days yellow rhombohedral crystals formed. The crystals obtained were suitable for single-crystal X-ray diffraction.

4. Conclusions

Four new Co^{II}, Ni^{II}, Zn^{II}, and Cu^{II} metal complexes with a prospective anti-TB drug (*E/Z*)-N′-((5-Hydroxy-3,4-bis(hydroxymethyl)-6-methylpyridin-2-yl)methylene)-isonicotin-ohydrazide (**LH**) were synthesized and characterized. Only one crystalline complex with copper(II) was obtained, consisting of two 1D polymer chains, whose coordination environment is completely abnormal for this type of complex. The other three metals formed

amorphous phases. Despite this, they were characterized by IR spectroscopy and mass spectrometry, and it was found that in all cases the coordination of the ligand is different. Thus, Ni^{II} forms a mono-complex, Co^{II} forms a *bis*-complex, but Zn^{II} can form mono- and tetra-nuclear complexes. According to infrared spectroscopy, Ni^{II} and Zn^{II} probably have similar solid-state structures because the vibrations correlate very well with each other. Cu^{II} and Co^{II} have individual vibrational patterns with the C=O vibrations missing in the case of copper(II) and remaining in the case of cobalt(II). The structure and energy of different conformational and spatial isomers were determined by DFT calculations, including the influence of the solvent. The *Z*-isomer of the corresponding ligand with intramolecular hydrogen bonds appeared to be the most stable; however, it is not able to coordinate copper(II) in the way that it occurs in the crystal packing, indicating isomeric conversions during synthesis. It can be assumed that **L**H can act as a Cu^{II} sensor in solution.

References

1. Popiołek, Ł. Hydrazide–Hydrazones as Potential Antimicrobial Agents: Overview of the Literature since 2010. *Med. Chem. Res.* **2017**, *26*, 287–301. [CrossRef] [PubMed]
2. Patole, J.; Sandbhor, U.; Padhye, S.; Deobagkar, D.N.; Anson, C.E.; Powell, A. Structural Chemistry and In Vitro Antitubercular Activity of Acetylpyridine Benzoyl Hydrazone and Its Copper Complex against Mycobacterium Smegmatis. *Bioorg. Med. Chem. Lett.* **2003**, *13*, 51–55. [CrossRef] [PubMed]
3. Dos Santos Fernandes, G.F.; De Souza, P.C.; Moreno-Viguri, E.; Santivañez-Veliz, M.; Paucar, R.; Pérez-Silanes, S.; Chegaev, K.; Guglielmo, S.; Lazzarato, L.; Fruttero, R.; et al. Design, Synthesis, and Characterization of N-Oxide-Containing Heterocycles with in Vivo Sterilizing Antitubercular Activity. *J. Med. Chem.* **2017**, *60*, 8647–8660. [CrossRef] [PubMed]
4. Oliveira, P.F.M.; Guidetti, B.; Chamayou, A.; André-Barrès, C.; Madacki, J.; Korduláková, J.; Mori, G.; Orena, B.S.; Chiarelli, L.R.; Pasca, M.R.; et al. Mechanochemical Synthesis and Biological Evaluation of Novel Isoniazid Derivatives with Potent Antitubercular Activity. *Molecules* **2017**, *22*, 1457. [CrossRef]
5. Hu, Y.Q.; Zhang, S.; Zhao, F.; Gao, C.; Feng, L.S.; Lv, Z.S.; Xu, Z.; Wu, X. Isoniazid Derivatives and Their Anti-Tubercular Activity. *Eur. J. Med. Chem.* **2017**, *133*, 255–267. [CrossRef]
6. Martins, F.; Santos, S.; Ventura, C.; Elvas-Leitão, R.; Santos, L.; Vitorino, S.; Reis, M.; Miranda, V.; Correia, H.F.; Aires-De-Sousa, J.; et al. Design, Synthesis and Biological Evaluation of Novel Isoniazid Derivatives with Potent Antitubercular Activity. *Eur. J. Med. Chem.* **2014**, *81*, 119–138. [CrossRef]
7. Solomon, E.I.; Heppner, D.E.; Johnston, E.M.; Ginsbach, J.W.; Cirera, J.; Qayyum, M.; Kieber-Emmons, M.T.; Kjaergaard, C.H.; Hadt, R.G.; Tian, L. Copper Active Sites in Biology. *Chem. Rev.* **2014**, *114*, 3659–3853. [CrossRef]

8. Brückmann, T.; Becker, J.; Würtele, C.; Seuffert, M.T.; Heuler, D.; Müller-Buschbaum, K.; Weiß, M.; Schindler, S. Characterization of Copper Complexes with Derivatives of the Ligand (2-Aminoethyl)Bis(2-Pyridylmethyl)Amine (Uns-Penp) and Their Reactivity towards Oxygen. *J. Inorg. Biochem.* **2021**, *223*, 111544. [CrossRef]

9. Serov, N.Y.; Shtyrlin, V.G.; Bukharov, M.S.; Ermolaev, A.V.; Gilyazetdinov, E.M.; Urazaeva, K.V.; Rodionov, A.A. Complex Structures, Formation Thermodynamics and Substitution Reaction Kinetics in the Copper(II)–Glycylglycyl-l-Tyrosine–l/d-Histidine Systems. *Polyhedron* **2022**, *228*, 116176. [CrossRef]

10. Murekhina, A.E.; Yarullin, D.N.; Sovina, M.A.; Kitaev, P.A.; Gamov, G.A. Copper (II)-Catalyzed Oxidation of Ascorbic Acid: Ionic Strength Effect and Analytical Use in Aqueous Solution. *Inorganics* **2022**, *10*, 102. [CrossRef]

11. Zavalishin, M.N.; Gamov, G.A.; Pimenov, O.A.; Pogonin, A.E.; Aleksandriiskii, V.V.; Usoltsev, S.D.; Marfin, Y.S. Pyridoxal 5′-Phosphate 2-Methyl-3-Furoylhydrazone as a Selective Sensor for Zn^{2+} Ions in Water and Drug Samples. *J. Photochem. Photobiol. A Chem.* **2022**, *432*, 114112. [CrossRef]

12. Santiago, P.H.O.; Santiago, M.B.; Martins, C.H.G.; Gatto, C.C. Copper(II) and Zinc(II) Complexes with Hydrazone: Synthesis, Crystal Structure, Hirshfeld Surface and Antibacterial Activity. *Inorg. Chim. Acta* **2020**, *508*, 119632. [CrossRef]

13. Kenđel, A.; Miljanić, S.; Kontrec, D.; Soldin, Ž.; Galić, N. Copper(II) Complexes of Aroylhydrazones: Preparation and Structural Characterization. *J. Mol. Struct.* **2020**, *1207*, 127783. [CrossRef]

14. Kovalenko, A.; Rublev, P.O.; Tcelykh, L.O.; Goloveshkin, A.S.; Lepnev, L.S.; Burlov, A.S.; Vashchenko, A.A.; Marciniak, L.; Magerramov, A.M.; Shikhaliyev, N.G.; et al. Lanthanide Complexes with 2-(Tosylamino)-Benzylidene-N-(Aryloyl)Hydrazones: Universal Luminescent Materials. *Chem. Mater.* **2019**, *31*, 759–773. [CrossRef]

15. Paschalidis, D.G.; Tossidis, I.A.; Gdaniec, M. Synthesis, Characterization and Spectra of Lanthanide(III) Hydrazone Complexes: The X-Ray Molecular Structures of the Erbium(III) Complex and the Ligand. *Polyhedron* **2000**, *19*, 2629–2637. [CrossRef]

16. Zhernakov, M.A.; Sedykh, A.E.; Becker, J.; Maxeiner, M.; Müller-Buschbaum, K.; Shtyrlin, V.G. Three Ytterbium(III) Complexes with Aromatic N-Donors: Synthesis, Structure, Photophysical Properties and Thermal Stability. *Z. Für Anorg. Und Allg. Chem.* **2022**, *648*, e202200230. [CrossRef]

17. Huang, W. {μ-1,5-Bis[(E)-1-(2-Pyrid-Yl)Ethyl-Idene]Carbonohydrazidato(1-)} Bis-[Chlorido-Methano-Lcopper(II)] Perchlorate. *Acta Crystallogr. Sect. E Struct. Rep. Online* **2009**, *65*, m1347. [CrossRef]

18. Wang, L.H.; Qiu, X.Y.; Liu, S.J. Synthesis, Characterization and Crystal Structures of Copper(II), Zinc(II) and Vanadium(V) Complexes, Derived from 3-Methyl-N′-(1-(Pyridin-2-Yl)Ethylidene)Benzohydrazide, with Antibacterial Activity. *J. Coord. Chem.* **2019**, *72*, 962–971. [CrossRef]

19. Emami, M.; Shahroosvand, H.; Bikas, R.; Lis, T.; Daneluik, C.; Pilkington, M. Synthesis, Study, and Application of Pd(II) Hydrazone Complexes as the Emissive Components of Single-Layer Light-Emitting Electrochemical Cells. *Inorg. Chem.* **2021**, *60*, 982–994. [CrossRef] [PubMed]

20. Badiger, D.S.; Hunoor, R.S.; Patil, B.R.; Vadavi, R.S.; Mangannavar, C.V.; Muchchandi, I.S.; Patil, Y.P.; Nethaji, M.; Gudasi, K.B. Synthesis, Spectroscopic Properties and Biological Evaluation of Transition Metal Complexes of Salicylhydrazone of Anthranilhydrazide: X-Ray Crystal Structure of Copper Complex. *Inorg. Chim. Acta* **2012**, *384*, 197–203. [CrossRef]

21. Ogunniran, K.O.; Mesubi, M.A.; Raju, K.V.S.N.; Narender, T. Structural and in Vitro Anti-Tubercular Activity Study of (E)-N′-(2,6-Dihydroxybenzylidene)Nicotinohydrazide and Some Transition Metal Complexes. *J. Iran. Chem. Soc.* **2015**, *12*, 815–829. [CrossRef]

22. Kuranova, N.N.; Yarullin, D.N.; Zavalishin, M.N.; Gamov, G.A. Complexation of Gold(III) with Pyridoxal 5′-Phosphate-Derived Hydrazones in Aqueous Solution. *Molecules* **2022**, *27*, 7346. [CrossRef]

23. Shtyrlin, N.V.; Khaziev, R.M.; Shtyrlin, V.G.; Gilyazetdinov, E.M.; Agafonova, M.N.; Usachev, K.S.; Islamov, D.R.; Klimovitskii, A.E.; Vinogradova, T.I.; Dogonadze, M.Z.; et al. Isonicotinoyl Hydrazones of Pyridoxine Derivatives: Synthesis and Antimycobacterial Activity. *Med. Chem. Res.* **2021**, *30*, 952–963. [CrossRef]

24. Gamov, G.A.; Zavalishin, M.N.; Petrova, M.V.; Khokhlova, A.Y.; Gashnikova, A.V.; Kiselev, A.N.; Sharnin, V.A. Interaction of Pyridoxal-Derived Hydrazones with Anions and Co^{2+}, Co^{3+}, Ni^{2+}, Zn^{2+} Cations. *Phys. Chem. Liq.* **2020**, *59*, 666–678. [CrossRef]

25. Alsharif, M.A.; Naeem, N.; Mughal, E.U.; Sadiq, A.; Jassas, R.S.; Kausar, S.; Altaf, A.A.; Zafar, M.N.; Mumtaz, A.; Obaid, R.J.; et al. Experimental and Theoretical Insights into the Photophysical and Electrochemical Properties of Flavone-Based Hydrazones. *J. Mol. Struct.* **2021**, *1244*, 130965. [CrossRef]

26. Bersuker, I.B. Modern Aspects of the Jahn-Teller Effect Theory and Applications to Molecular Problems. *Chem. Rev.* **2001**, *101*, 1067–1114. [CrossRef] [PubMed]

27. Brückmann, T.; Becker, J.; Turke, K.; Smarsly, B.; Weiß, M.; Marschall, R.; Schindler, S. Immobilization of a Copper Complex Based on the Tripodal Ligand (2-Aminoethyl)Bis(2-Pyridylmethyl)Amine (Uns-Penp). *Z. Für Anorg. Und Allg. Chem.* **2021**, *647*, 560–571. [CrossRef]

28. Stumpf, T.D.J.; Steinbach, M.; Würtele, C.; Becker, J.; Becker, S.; Fröhlich, R.; Göttlich, R.; Schindler, S. Reactivity of Copper Complexes with Bis(Piperidinyl)Methane and Bis(Quinolinyl)Methane Ligands. *Eur. J. Inorg. Chem.* **2017**, *2017*, 4246–4258. [CrossRef]

29. Shtyrlin, V.G.; Zakharov, A.V.; Evgenieva, I.I. The Nature of the "Pentaamine Effect" and the Reactivity of Copper(II) Pentacoordination Compounds. *J. Inorg. Chem.* **1983**, *28*, 435–441. (In Russian)

30. Powell, D.H.; Helm, L.; Merbach, A.E. ^{17}O Nuclear Magnetic Resonance in Aqueous Solutions of Cu^{2+}: The Combined Effect of Jahn–Teller Inversion and Solvent Exchange on Relaxation Rates. *J. Chem. Phys.* **1991**, *95*, 9258. [CrossRef]

31. Bruno, I.J.; Cole, J.C.; Kessler, M.; Luo, J.; Momerwell, W.D.S.; Purkis, L.H.; Smith, B.R.; Taylor, R.; Cooper, R.I.; Harris, S.E.; et al. Retrieval of Crystallographically-Derived Molecular Geometry Information. *J. Chem. Inf. Comput. Sci.* **2004**, *44*, 2133–2144. [CrossRef]

32. Sutradhar, M.; Roy Barman, T.; Alegria, E.C.B.A.; Guedes Da Silva, M.F.C.; Liu, C.M.; Kou, H.Z.; Pombeiro, A.J.L. Cu(II) Complexes of N-Rich Aroylhydrazone: Magnetism and Catalytic Activity towards Microwave-Assisted Oxidation of Xylenes. *Dalt. Trans.* **2019**, *48*, 12839–12849. [CrossRef]

33. Rowland, J.M.; Olmstead, M.M.; Mascharak, P.K. Monomeric and Dimeric Copper(II) Complexes of a Novel Tripodal Peptide Ligand: Structures Stabilized via Hydrogen Bonding or Ligand Sharing. *Inorg. Chem.* **2000**, *39*, 5326–5332. [CrossRef]

34. Sauer, D.C.; Wadepohl, H. Variable Coordination Modes of an Active Ligand Periphery in 1,3-Bis(2-Pyridylimino)Isoindolato Copper(II) Complexes. *Polyhedron* **2014**, *81*, 180–187. [CrossRef]

35. Chetana, P.R.; Rao, R.; Saha, S.; Policegoudra, R.S.; Vijayan, P.; Aradhya, M.S. Oxidative DNA Cleavage, Cytotoxicity and Antimicrobial Studies of l-Ornithine Copper (II) Complexes. *Polyhedron* **2012**, *48*, 43–50. [CrossRef]

36. Xu, C.; Mao, H.; Shen, X.; Zhang, H.; Liu, H.; Wu, Q.; Hou, H.; Zhu, Y. Synthesis and Crystal Structures of Cu(II) and Pb(II) Aroylhydrazone Complexes and Magnetic Properties of $[Cu_2(L)_2(Cl)_2(HO)_6]_n$ (HL=2-Pyridylaldehyde Isonicotinoylhydrazone). *J. Coord. Chem.* **2007**, *60*, 193–200. [CrossRef]

37. Murphy, T.B.; Rose, N.J.; Schomaker, V.; Aruffo, A. Syntheses of Iron(III) Aroyl Hydrazones Containing Pyridoxal and Salicylalde-hyde. The Crystal and Molecular Structure of Two Iron(III)-Pyridoxal Isonicotinoyl Hydrazone Complexes. *Inorg. Chim. Acta* **1985**, *108*, 183–194. [CrossRef]

38. Bukharov, M.S.; Shtyrlin, V.G.; Gilyazetdinov, E.M.; Serov, N.Y.; Madzhidov, T.I. Hydration of Copper(II) Amino Acids Complexes. *J. Comput. Chem.* **2018**, *39*, 821–826. [CrossRef] [PubMed]

39. Bukharov, M.S.; Shtyrlin, V.G.; Mamin, G.V.; Stapf, S.; Mattea, C.; Mukhtarov, A.S.; Serov, N.Y.; Gilyazetdinov, E.M. Structure and Dynamics of Solvation Shells of Copper(II) Complexes with N,O-Containing Ligands. *Inorg. Chem.* **2015**, *54*, 9777–9784. [CrossRef] [PubMed]

40. Bukharov, M.S.; Shtyrlin, V.G.; Mukhtarov, A.S.; Mamin, G.V.; Stapf, S.; Mattea, C.; Krutikov, A.A.; Il'In, A.N.; Serov, N.Y. Study of Structural and Dynamic Characteristics of Copper(II) Amino Acid Complexes in Solutions by Combined EPR and NMR Relaxation Methods. *Phys. Chem. Chem. Phys.* **2014**, *16*, 9411–9421. [CrossRef]

41. Neese, F. The ORCA Program System. *Wiley Interdiscip. Rev. Comput. Mol. Sci.* **2012**, *2*, 73–78. [CrossRef]

42. Kohn, W.; Becke, A.D.; Parr, R.G. Density Functional Theory of Electronic Structure. *J. Phys. Chem.* **1996**, *100*, 12974–12980. [CrossRef]

43. Sheldrick, G.M. SHELXT-Integrated Space-Group and Crystal-Structure Determination. *Acta Crystallogr. Sect. A Found. Crystallogr.* **2015**, *71*, 3–8. [CrossRef] [PubMed]

44. Sheldrick, G.M. A Short History of SHELX. *Acta Crystallogr. Sect. A Found. Crystallogr.* **2008**, *64*, 112–122. [CrossRef]

45. Macrae, C.F.; Edgington, P.R.; McCabe, P.; Pidcock, E.; Shields, G.P.; Taylor, R.; Towler, M.; Van De Streek, J. Mercury: Visualization and Analysis of Crystal Structures. *J. Appl. Crystallogr.* **2006**, *39*, 453–457. [CrossRef]

46. Becke, A.D. Density-functional Thermochemistry. III. The Role of Exact Exchange. *J. Chem. Phys.* **1998**, *98*, 5648. [CrossRef]

47. Lee, C.; Yang, W.; Parr, R.G. Development of the Colle-Salvetti Correlation-Energy Formula into a Functional of the Electron Density. *Phys. Rev. B* **1988**, *37*, 785. [CrossRef]

48. Schäfer, A.; Huber, C.; Ahlrichs, R. Fully Optimized Contracted Gaussian Basis Sets of Triple Zeta Valence Quality for Atoms Li to Kr. *J. Chem. Phys.* **1998**, *100*, 5829. [CrossRef]

49. Weigend, F.; Häser, M.; Patzelt, H.; Ahlrichs, R. RI-MP2: Optimized Auxiliary Basis Sets and Demonstration of Efficiency. *Chem. Phys. Lett.* **1998**, *294*, 143–152. [CrossRef]

50. Weigend, F.; Ahlrichs, R. Balanced Basis Sets of Split Valence, Triple Zeta Valence and Quadruple Zeta Valence Quality for H to Rn: Design and Assessment of Accuracy. *Phys. Chem. Chem. Phys.* **2005**, *7*, 3297–3305. [CrossRef] [PubMed]

51. Cossi, M.; Rega, N.; Scalmani, G.; Barone, V. Energies, Structures, and Electronic Properties of Molecules in Solution with the C-PCM Solvation Model. *J. Comput. Chem.* **2003**, *24*, 669–681. [CrossRef] [PubMed]

52. Grimme, S.; Antony, J.; Ehrlich, S.; Krieg, H. A Consistent and Accurate Ab Initio Parametrization of Density Functional Dispersion Correction (DFT-D) for the 94 Elements H-Pu. *J. Chem. Phys.* **2010**, *132*, 154104. [CrossRef] [PubMed]

53. Grimme, S.; Ehrlich, S.; Goerigk, L. Effect of the Damping Function in Dispersion Corrected Density Functional Theory. *J. Comput. Chem.* **2011**, *32*, 1456–1465. [CrossRef] [PubMed]